Society For Biomaterials

Micro-CT and PET analysis of bone regeneration induced by biodegradable scaffolds as carriers for dental pulp stem cells in a rat model of calvarial "critical size" defect: Preliminary data

Susanna Annibali,[1*] Diana Bellavia,[2*] Livia Ottolenghi,[1] Andrea Cicconetti,[1] Maria Paola Cristalli,[1] Roberta Quaranta,[2] Andrea Pilloni[1]

[1]Department of Oral and Maxillofacial Sciences, "Sapienza" University of Rome, Rome, Italy
[2]Department of Molecular Medicine, "Sapienza" University of Rome, Rome, Italy

Received 26 March 2013; revised 10 September 2013; accepted 27 September 2013
Published online 21 October 2013 in Wiley Online Library (wileyonlinelibrary.com). DOI: 10.1002/jbm.b.33064

Abstract: Bone regeneration strategies in dentistry utilize biodegradable scaffolds seeded with stem cells able to induce bone formation. However, data on regeneration capacity of these tissue engineering constructs are still deficient. In this study micro-Computed tomography (micro-CT) and positron emission tomography (PET) analyses were used to investigate bone regeneration induced by two scaffolds [Granular deproteinized bovine bone (GDPB) and Beta-tricalcium phosphate (β-TCP)] used alone or in combination with dental pulp stem cells (DPSC) in a tissue engineered construct implanted in a rat critical calvarial defect. Bone mineral density (BMD) and standard uptake value (SUV) of tracer incorporation were measured after 2, 4, 8, and 12 weeks post-implant. The results showed that: (1) GDPB implants were mostly well positioned, as compared to ß-TCP; (2) GDPB induced higher BMD and SUV values within the cranial defect as compared to ß-TCP, either alone or in combination with stem cells; (3) addition of DPSC to the grafts did not significantly induce an increase in BMD and SUV values as compared to the scaffolds grafted alone, although a small tendency to increase was observed. Thus our study demonstrates that GDPB, when used to fill critical calvarial defects, induces a greater percentage of bone formation as compared to ß-TCP. Moreover, this study shows that addition of DPSC to pre-wetted scaffolds has the potential to ameliorate bone regeneration process, although the set of optimal conditions requires further investigation. © 2013 Wiley Periodicals, Inc. J Biomed Mater Res Part B: Appl Biomater, 102B: 815–825, 2014.

Key Words: stem cells, biomaterials, μ-CT, μ-PET, [18F]-NaF, bone regeneration

How to cite this article: Annibali S, Bellavia D, Ottolenghi L, Cicconetti A, Cristalli MR, Quaranta R, Pilloni A. 2014. Micro-CT and PET analysis of bone regeneration induced by biodegradable scaffolds as carriers for dental pulp stem cells in a rat model of calvarial "critical size" defect: Preliminary data. J Biomed Mater Res Part B 2014:102B:815–825.

INTRODUCTION

In dentistry the increasing number of surgical and restorative procedures related to either oral rehabilitation with the placement of dental implants and ceramic crowns or to periodontal regeneration have required the continuous development of successful methods such as the use of biomaterials for guided tissue/bone regeneration and grafting materials.[1,2]

Given the appositional nature of bone formation, bioactive biomaterials are desirable as tissue engineering scaffolds for their capability to mimic the natural environment of the extracellular matrix.[3] In addition, the advent of tissue engineering strategies with the incorporation of osteogenic-capable cells[4] has increased scaffold effectiveness and added further versatility to dental-implants-periodontal therapy.[5]

Mesenchymal stem cells (MSCs) represent an ideal cell population for scaffold-based tissue engineering[6–10] because, when cultured in scaffolds, they are capable of inducing *in vivo* new bone formation in critical-size defects of animal models.[11–14] It has been also shown that osteoblast-like cells derived from MSCs share characteristics similar to osteoblasts[15] and may secrete a good amount of matrix to form mature bone with deposition of calcium salts. Among MSC types used for scaffold-based tissue engineering, dental pulp stem cells (DPSCs) and periosteal stem cells (PeSC) represent ideal cell populations[16–19] because of their ability to differentiate into a variety of cell types including osteocytes.[20,21] In a previous study we determined bone regeneration properties of DPSC or PeSC when seeded with different scaffolds in a tissue-engineered construct.[22] We used two commercially available scaffolds (granular

Conceived and designed the experiments: SA, DB, LO. Performed the experiments: AC, MPC. Analyzed the data: LO, AP. Processed the stem cell culture: DB, RQ. Wrote the article: SA, AP.
*Both authors contributed equally to this work.
Correspondence to: S. Annibali (susanna.annibali@uniroma1.it)
Contract grant sponsor: Fondazione Roma

deproteinized bovine bone with 10% porcine collagen and granular beta-tricalcium phosphate) and one not yet introduced on the market (a sponge of agarose and nano-hydroxyapatite) and analyzed bone regeneration (measured as a percentage of bone volume on the total defect area) when they were used to fill critical calvarial defect in SCID BEIGE nude mice. However, our data showed that tissue-engineered constructs did not significantly improve bone-induced regeneration process when compared to the effect of scaffolds alone. Also, no significant differences among scaffolds were found. Our findings suggest that further studies are needed to evaluate the potential of DPSC and PeSC in tissue construct and identify the appropriate conditions to generate bone tissue in critical size defects. Thus there is the need to explore this issue with new technologies and diagnostic techniques, that may efficiently verify the effectiveness of new scaffold/stem cell combination to induce bone regeneration.

The micro-Computed tomography (micro-CT) analysis has become an important method of investigation in the evaluation of bone regeneration induced by scaffolds implanted into the bone defect.[23,24] The micro-CT allows to work on small laboratory animals in a noninvasive manner, in order to characterize the structure of the soft tissues and detect bone anomalies.[25] A normalized method of selecting a region of interest is required in order to study volumetric changes. Concerning bone scaffolds, micro-CT is employed to quantify scaffold geometry, newly formed bone, neovascularization, and prebone matrix.[26] Micro-CT at a spatial resolution of 16 μm has been used to study bone ingrowth within different scaffolds by Cartmell et al.[27] Micro-CT scans taken weekly between 4 and 8 weeks showed the increase of new bone volume. In addition, there has been recently a development of integrated tomographic imaging systems that can simultaneously acquire anatomical information (through an X-ray CT scan) and can perform molecular imaging studies of the above outlined type using targeted radiolabeled tracers and positron emission tomography (PET) imaging.[28] This dual-modality imaging system inherently produces accurate spatial registration of the two three-dimensional (3D) image volumes, because the same volume is being scanned by both imaging technologies at the same time.

Thus in this study we utilized micro-CT and PET analyses to investigate the regeneration capacity of two types of previously investigated biomaterials in nude immunodeficient rats [Granular deproteinized bovine bone (GDPB) and Beta-tricalcium phosphate (β-TCP)] used alone and in combination with DPSC in a tissue engineered construct implanted in two circular critical calvarial defect of each animal. This analysis provided information on the correct positioning of the substrate (scaffold) and on the quantification of bone regeneration by measuring bone mineral density (BMD) with micro-CT and standard uptake value of tracer incorporation with PET after 2, 4, 8, and 12 weeks after implant.

MATERIALS AND METHODS

Animals

NIH-RNU FOXN1 nude rats (50-day old) were purchased by Charles River Laboratories International (Wilmington, MA) and housed in the facilities of the Department of Histology and Medical Embryology of the "Sapienza" University of Rome. Rats ($n = 8$) were kept under standard conditions on a 12/12h dark/light cycle and were allowed access to water and food during acclimation *ad libitum*. Animals were maintained according to the guidelines for ethical conduct developed by the European Communities Council Directive of November 24, 1986 (86/609/EEC). The use of such specific strains of rats was decided because they do not show immune response due to the necessity of using human stem cells for bone regeneration. All efforts were made to minimize pain or discomfort of the animals.

Scaffolds

Granular deproteinized bovine bone (GDPB) (Geistlich Bio-Oss Collagen®, Geistlich Pharma North America, 202 Carnegie Center, Princeton, NJ) is a bone substitute of bovine origin made by bone granules with the addition of 10% highly purified porcine collagen with a porosity (250–1000 μm) and crystal size very similar to human bone. Beta-tricalcium phosphate (ß-TCP) (Synthograft™, Bicon Dental Implants, 501 Arborway, Boston, MA) an FDA approved grafting material, is a pure synthetic biocompatible, and resorbable granulate ceramic material with a pore size of 50–500 μm. Selection of scaffolds was made on a translational perspective scaffold-based bone tissue engineering therapies to clinical use.

In vitro cell culture

Dental pulp stem cells (DPSCs) were isolated from deciduous and permanent human teeth.[29] Within 24 h, red blood cells and other non-adherent cells were removed and fresh medium was added to favour the growth of adherent stem cells. The cells were allowed to reach ~80% confluence. For passaging, they were washed out with PBS and detached by incubating with 0.05% trypsin-EDTA 0.02% in PBS solution (EuroClone®) for 5–10 min at 37°C. Stem cells were replated in a new 75cm2 flask with an appropriate dilution.[30]

We characterized primary cell lines of DPSCs by using specific stem cells markers, such as Nanog and Oct-4 (POU class 5 homeobox 1) by RT-PCR (for primers used see Karaoz[30]) and immunofluorescence. We also analyzed the expression of CD146, a pericyte marker that is one of the most commonly reported positive cell surface markers on mesenchymal cells,[31] by flow cytometry (FACS-Calibur, BD Biosciences) using an α-CD146 antibody (BD PharmingenTM).

Differentiated cells towards osteoblastic phenotype were obtained by treatment with 100 μ*M* L-ascorbic acid (Sigma),[29] added every day in the culture medium, and 20 vol % of FBS in the α-MEM medium, since is well-known that FBS exerts a differentiation activity favoring osteoblastic differentiation when used in high percentage.[32] The cells were treated 10–15 days before using them to seed the scaffolds. The osteogenic commitment was identified by the expression of specific markers, such as osteonectin, and runx2 (runt-related transcription factor 2) genes by RT-PCR (for primers used see Karaoz[30]).

Scaffold preparation

When a sufficient cell number was obtained, DPSCs were trypsinized and washing in culture medium and seeded onto the scaffolds. A block of granular deproteinized bovine bone was placed in a 24-well plates, while for beta-tricalcium phosphate an amount of granulate was distributed in each well of a 96-well plate. Both of them were pre-wetted before adding the cells through an overnight incubation in culture medium at 37°C. The cells, after the treatment with 20 vol % of FBS and 100 μ*M* L-ascorbic acid, were seeded onto the scaffolds at a density of 0.5–1 × 106 cells/scaffold. After 1 h, 1 mL of medium was added to the GDPB. The *in vitro* cell constructs were cultured in osteogenic inducing medium for 4 days in a humidified atmosphere at 37°C containing 5% CO_2 before implantation into cranial defect.

In vivo cranial defect

Two bilateral critical-size circular defects (5 mm diameter; 1 mm thickness) were created using a hand drill and trephine bit in the parietal bones of the skull on either side of the sagittal suture line. Care was taken to avoid damage to the sagittal suture or to interrupt the *dura mater* beneath the bone. During the procedure, sterile saline was dripped over the drilling site in order to avoid extensive heating and to protect the brain. Surgery was performed under general anesthesia (xylazine:ketamine, 1:1 solution in saline) by intraperitoneal injection.

Experimental groups

Each animal received different combinations of biomaterial and stem cells to fill the two defects. The animals were divided into two experimental groups ($n = 4$ animals/group), which received the following implants: (1) scaffolds seeded with stem cells (1×10^6 DPSC); (2) scaffold without cells. A total of eight animals were used in four experimental groups generated by the combination of biomaterial and stem cells: β-TCP (β); β-TCP/DPSC (β/C); GDPB (G) and GDPB/DPSC (G/C). After 2, 4, 8, and 12 weeks post-surgery animals underwent to μ-PET/CT analyses and body weight was recorded.

Micro-computed tomography (μ-CT)

The μ-CT projection images were acquired at 80 kVp, 450 mA and a resolution of 90 μm. The μ-CT images were reconstructed to give a volume data set.

The kVp and exposure time were kept consistent for all samples. The 2D projections acquired were elaborated to generate the volume of interest. Using the software MicroView—Advanced Bone Analysis (ABA) we evaluated the osteogenic properties of the biomaterial (alone or associated with DPSC) in the bone defect. For comparison we used the bone mineral density (BMD), an index parameter of bone mineralization expressed in mg/cm^3.

This quantitative analysis consisted of several steps:

1. Analysis of BMD of GDPB and β-TCP not implanted in the defect, in order to have a reference control. Values of BMD for GDPB and β-TCP were obtained by drawing 10 regions of interest (ROIs) with an isovolume of 0.10 mm^3. The ABA software allowed the calculation of the BMD and the data shown represent the mean obtained from the selected ROIs.
2. Evaluation of the correct positioning of biomaterial within the bone defect. To perform this analysis μ-CT acquired images were used.
3. Analysis of BMD of scaffolds implanted in cranial defects. This examination was carried out following two protocols:
   a. By manually drawing ROIs of isovolume (9.56 ± 0.36 mm^3) including only the biomaterial positioned into the defect. Thus, the defect area was "ideally" represented as a cylinder with 5.0 mm diameter and 0.5 mm biomaterial thickness. The following formula to calculate the cylinder volume at each time analysis (V) was used: $V = (\pi r^2) \times h$, where "r^2" is the radius of the circle represented by the defect and "h" is the height of the grafted biomaterial.
   b. By manually drawing ROIs (n°. 10) of isovolume (0.10 mm^3) and including the biomaterial also positioned outside the defect area. This type of analysis was made in order to evaluate the BMD regardless the position of the biomaterial. In fact, in the previous analysis (a), the software evaluated BMD into the defect, including empty areas where the biomaterial was absent or displaced (Table I). By measuring BMD in these "empty" areas, a lower BMD value was obtained. To avoid this problem, in this second step only the areas of maximal biomaterial density were evaluated. In this way, the data obtained reflect more properly the amount of graft-induced osteogenesis.

TABLE I. The Position of the Implanted Material Within the Cranial Defect

ID	Right Cranial Defect Implant	Left Cranial Defect Implant
1A	Absent/displaced	Absent/displaced Absent/displaced
2A	Absent/displaced	Present/slightly displaced
3A	Absent/displaced	Absent/displaced
4A	Absent/displaced	
1B	Present/correctly placed	Present/slightly displaced
2B	Present/correctly placed	Present/slightly displaced
3B	Present/correctly placed	Present/slightly displaced
4B	Present/correctly placed	Present/correctly placed

A total of four experimental groups were generated by the combination of biomaterials and stem cells: β-TCP (β); β-TCP/DPSC (β/C); GDPB (G) and GDPB/DPSC (G/C). ID = identification number. A (β-TCP-based implants); B (GDPB -based implants). β-TCP: Beta-tricalcium phosphate; GDPB: granular deproteinized bovine bone; DPSC: dental pulp stem cells. Absent/displaced = material not detectable due to displacement from the defect site or reabsorption; Present/correctly placed = material correctly positioned into the defect site; Present/slightly displaced = detectable material either inside or outside the defect site.

FIGURE 1. μ-CT images showing the positioning of the graft in the cranial defects of the beta-tricalcium phosphate group (group A) at 2-weeks post implant.

For this data analysis only samples from the group B (GDPB) were used.

Positron emission tomography (μ-PET)

PET imaging was performed in spontaneously breathing rats under isoflurane anesthesia (2% isoflurane, 98% oxygen). Production of the injection solution (sterile and pyrogen-free) of [18F]—sodium fluoride ([18F]-NaF) tracer was carried out at pharmaceutical NSA Srl. After purification and pH adjustment, a solution ready for injection was obtained. The radiotracer was dispensed intravenously, through injection into the tail vein after anesthesia. The animals were monitored to analysis PET/CT. The vital functions of animals were continuously monitored to ensure animals welfare during each experimental phase. Rats were fasted for 8 h and then subjected to 15-min static scan after 40 min the radiotracer injection. The scanning region was placed exclusively on the head of the animals. The PET scans were reconstructed using the ordered subset expectation maximization (OSEM) algorithm. The μ-PET imaging was performed using Explore Vista (General Electric Healthcare), a tomograph for small laboratory animals (mice and rats). The PET study was only performed after 4 and 12 weeks postsurgery.

FIGURE 2. μ-CT images showing the positioning of the graft in the cranial defects of the granular deproteinized bovine bone (group B) at 2-weeks post implant (see Table I for details).

μ-PET/CT integration analysis

PET/CT data integration was performed with an integrated PET/CT processing and fusion console (Advantage Windows 4.5, GE). With this console it was possible, for each animal, to draw ROIs of the districts of interest. 1.0 mm^3 ROIs ($n = 20$) were drawn for each bone defect to allow a precise analysis inside and outside the defect:

In addition, for each animal ROIs at the level of the parietal bone and at the parietal bone suture were drawn, in order to make a comparison. This method allowed extrapolating the following quantitative data on tracer uptake in the regions of interest:

1. *SUV max* (maximum standard uptake value), defined as the highest uptake value in each volume unit (voxel) of the ROI;
2. *SUV*, a non dimensional and semiquantitative value representing the mean SUV value found in the ROI.

Statistical analysis

Data were analyzed by two-way analysis of variance (ANOVA) considering treatments and time as variables. Differences between groups of treatment were analyzed by one-way

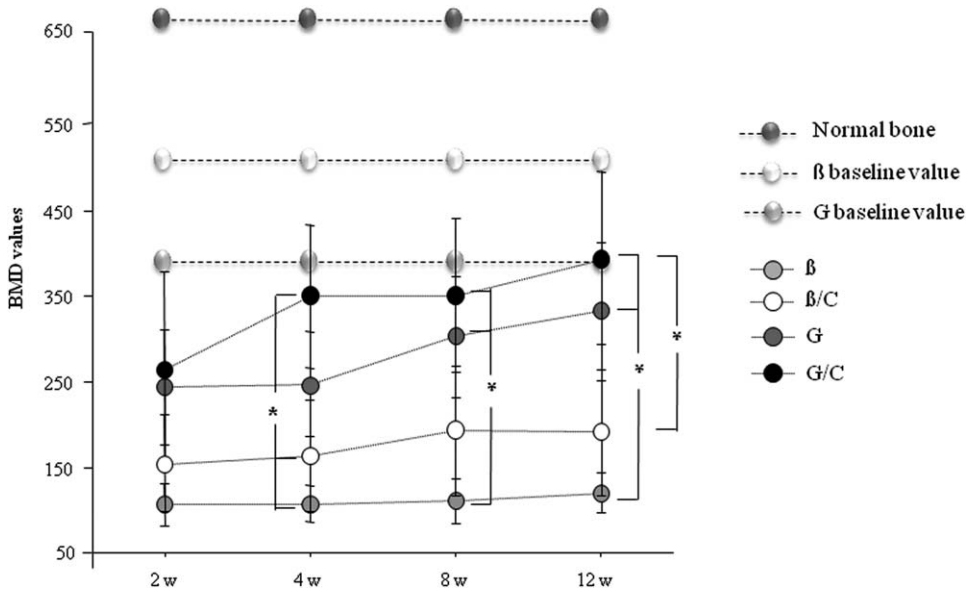

FIGURE 3. Bone mineral density (BMD) obtained from the μ-CT analysis in the bone defect at 2, 4, 8, and 12 weeks (w) post-surgery in the four experimental groups: β-TCP (β); β-TCP/DPSC (β/C); GDPB (G) and GDPB/DPSC (G/C). Data represent means ± S.E.M. β-TCP: Beta-tricalcium phosphate; GDPB: Granular deproteinized bovine bone; DPSC: dental pulp stem cells.

(ANOVA) followed by Fisher's protected least significant difference (PLSD) post-hoc test. A P value <0.05 was considered statistically significant. Statistical analysis was performed using the Statview software from SAS Institute.

RESULTS

Body weight

Body weight was recorded at each time points (weeks) and no significant differences were found between the experimental groups.

Micro-CT (μ-CT) analysis

Evaluation of correct positioning of the graft implanted in the cranial defect. μ-CT was performed at 2, 4, 8, and 12 weeks post-surgery. Analyzing μ-CT images, a preliminary evaluation of the positioning of scaffold was made. Table I shows the position of the implanted material. As shown in the table, β-TCP grafts (Group A) were absent or not correctly positioned in the bone defects, while GDPB (Group B) was generally correctly positioned. Figures 1 and 2 show the actual position of the grafted material.

Bone mineral density (*BMD*) within the defect area. Before data extrapolation of quantitative grafted biomaterial in cranial defects, bone mineral density (BMD) of the scaffolds (alone and not implanted into the bone defect) and the normal calvarial bone was evaluated in order to have baseline values for comparison. BMD values for β-TCP and GDPB (expressed in mg/cm^3) were 518.70 and 385.81, respectively. BMD value of normal cortical bone was 661.6.

Figure 3 shows the BMD obtained from the μ-CT analysis in the bone defect at 2, 4, 8, and 12 weeks post-surgery in the experimental groups. This analysis was made on the scaffold exclusively present within the bone defect and considering a constant volume of 9.56 mm^3 Two-ways ANOVA showed that there was a time effect ($P < 0.05$), because BMD values increased from 2 to 12 weeks in all experimental groups. One-way ANOVA showed a significant effect of the treatment at 4, 8, and 12 weeks post-surgery ($Ps < 0.05$). Post-hoc analysis showed that at 4 weeks BMD values of GDPB/DPSC (G/C) were higher than those of β-TCP ($P < 0.05$) and β-TCP/DPSC ($P < 0.05$). At 8 ($Ps < 0.05$) and 12 ($Ps < 0.05$) weeks we found that GDPB induced a higher amount of BMD within the cranial defect as compared to β-TCP, either alone or in combination with stem cells. Moreover, addition of stem cells induced a slight, although not statistically significant, increase of BMD values in both groups as compared to the scaffold grafted alone. The BMD β-TCP and GDPB baseline values were higher than those of the scaffolds implanted in the cranial defects.

Bone mineral density (*BMD*) of the graft implanted in the areas of bone formation maximal density. The BMD of the graft implanted in the areas of maximal density of bone formation was evaluated samples from the group B (GDPB) (Figure 4). Two-ways ANOVA showed a significant effect of time ($P < 0.001$), because BMD values increased from 2 to 12 weeks in all groups. We found that in the GDPB group the mean of BMD increases from T2 (360.15 mg/cm^3) to T12 (416.70 mg/cm^3). The BMD in the group GDPB/DPSC increases from T2 (460.44 mg/cm^3) to T12 (513.58 mg/cm^3). The BMD of the GDPB baseline (385.81 mg/cm^3) is lower than that found in the scaffold grafted alone or in combination with DPSC at 8 and 12 weeks post-implantation.

No significant differences between GDPB and GDPB/DPSC were evidenced at all time points. That is to say that

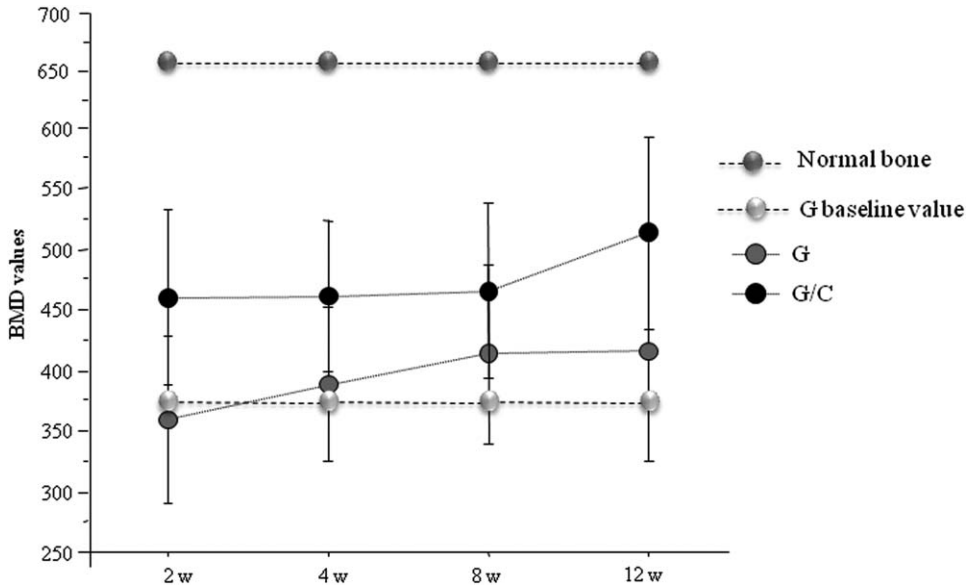

FIGURE 4. Bone mineral density (BMD) in the areas of maximal density of bone formation, regardless of the location of the grafted material (GDPB). Only samples from the group B (GDPB) were used. BMD were obtained from the μ-CT analysis in the bone defect at 2, 4, 8, and 12 weeks (w) post-surgery. Data represent means ± S.E.M. G: GDPB group; G/C: GDPB/DPSC group; GDPB: Granular deproteinized bovine bone; DPSC: dental pulp stem cells.

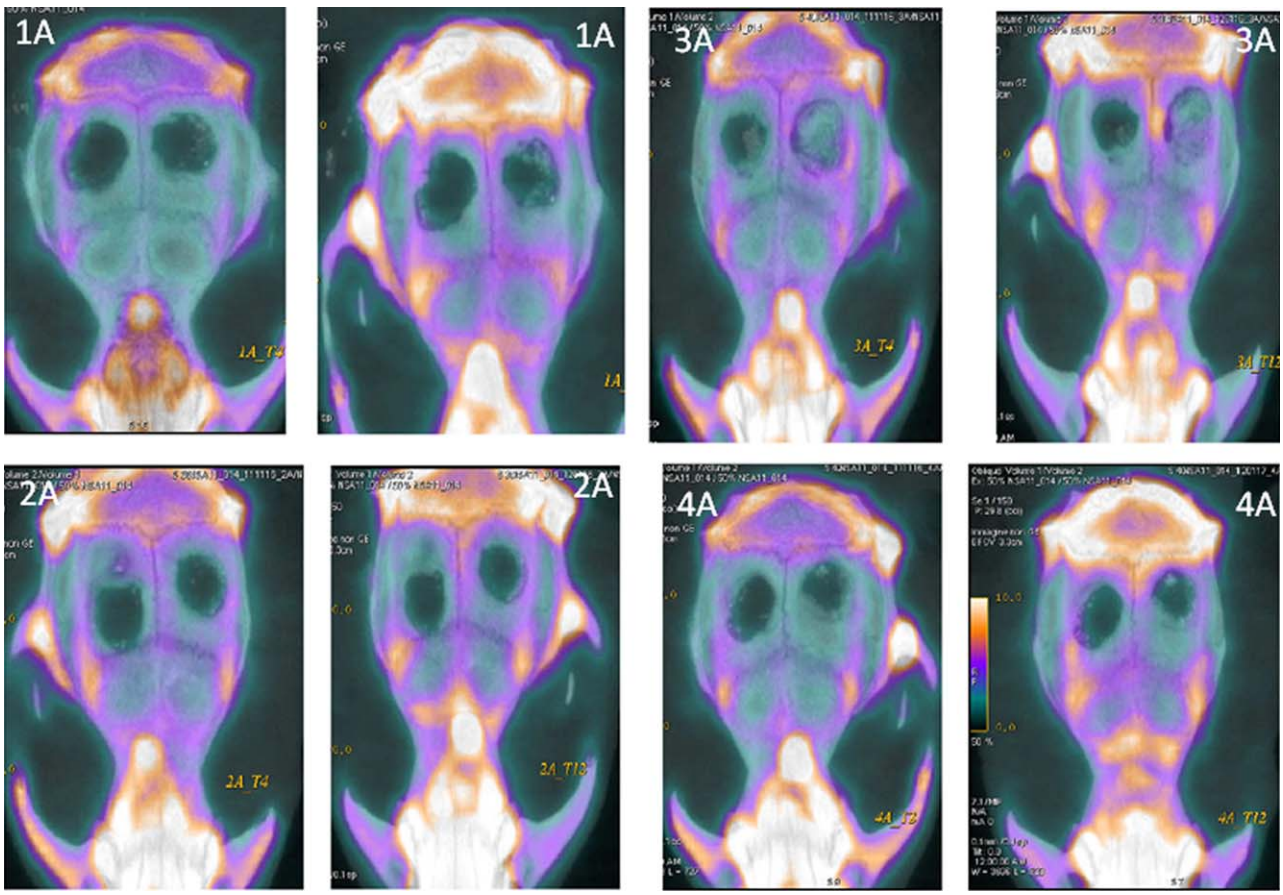

FIGURE 5. Integrated μ-PET/CT images for each animal of experimental group A (β-TCP; β-TCP/DPSC) after 4 (left side) and 12 (right side) weeks from graft (see Table I for details). ß-TCP: Beta-tricalcium phosphate; DPSC: dental pulp stem cells. [Color figure can be viewed in the online issue, which is available at wileyonlinelibrary.com.]

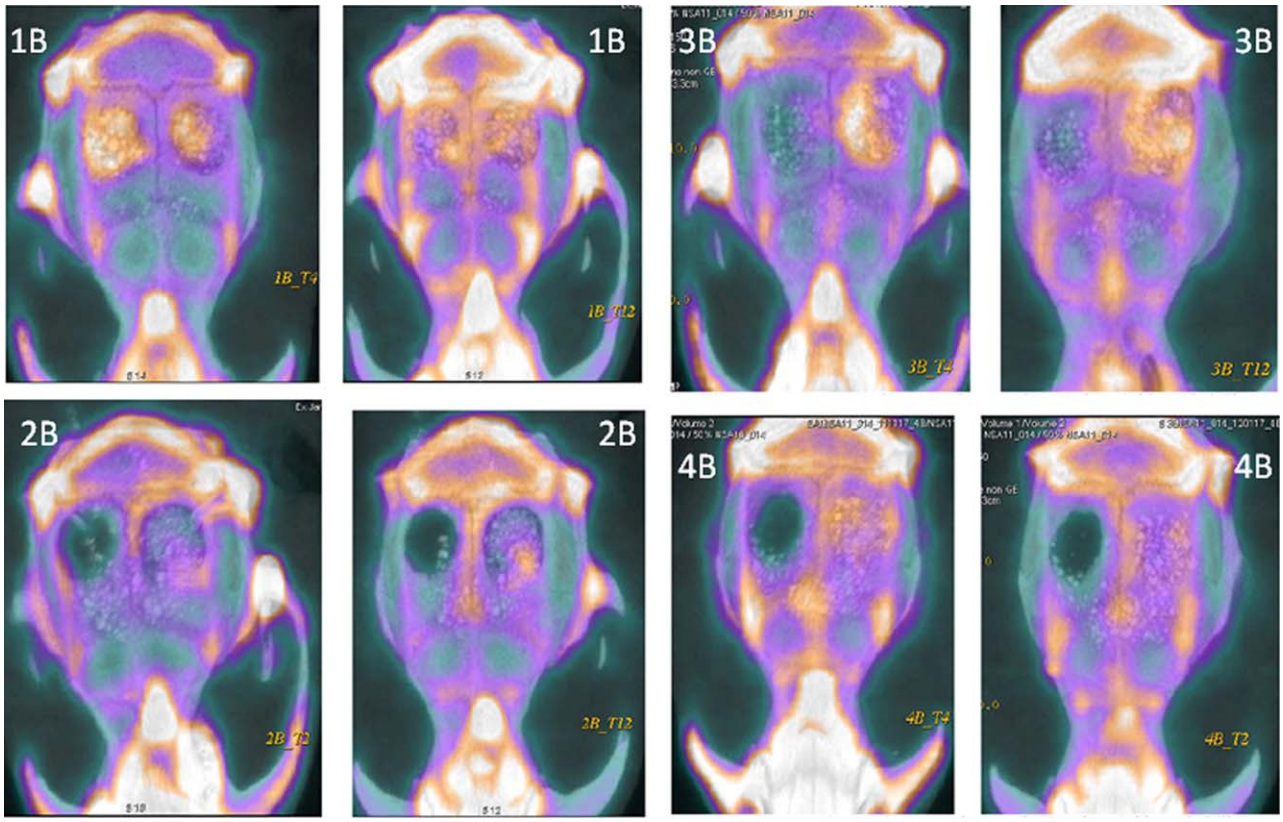

FIGURE 6. Integrated μ-PET/CT images for each animal of experimental group B (GDPB and GDPB/DPSC) after 4 (left side) and 12 (right side) weeks from graft (see Table I for details). GDPB: Granular deproteinized bovine bone; DPSC: dental pulp stem cells. [Color figure can be viewed in the online issue, which is available at wileyonlinelibrary.com.]

addition of stem cells did not increase new bone formation as compared to the scaffold alone.

μ-PET μ-PET/CT integration analysis

Integrated μ-PET/CT images for each animal of experimental groups are shown in Figures 5–7. Analysis [^{18}F]-NaF-PET provided information on the distribution of tracer within the bone defect, expressed as SUV and SUVmax. Biologically, ^{18}F-ions, after chemisorptions onto hydroxyapatite, exchange rapidly for OH on the surface of the hydroxyapatite matrix ($Ca_{10}(PO_4)_6OH_2$) to form fluoroapatite ($Ca_{10}(PO_4)_6F_2$) (18). The relationship between osteoblastic and osteoclastic activity determines the incorporation of ^{18}F-NaF into the bone matrix.

For each animal, the values of SUV and SUVmax were extrapolated from the quantitative analysis of images acquired at 4 and 12 weeks from graft implant (Figure 8). There were significant group effects in SUV ($P < 0.05$) and SUVmax ($P < 0.05$) because samples from β-TCP-based implants showed lower SUV and SUVmax values as compared to GDPB-based implants.

Post hoc analysis revealed that at 4 and 12 weeks the G/C group had significantly higher values of SUV and SUVmax as compared to β ($Ps < 0.05$) and β/C ($Ps < 0.05$) groups. At 12 weeks we also found that the G group had higher SUV ($Ps < 0.05$) and SUVmax ($Ps < 0.05$) as compared to the β group. Addition of stem cells did not significantly change SUV and SUV max as compared to the scaffolds grafted alone.

DISCUSSION

The aim of this study was to characterize bone regeneration induced by dental pulp stem cells (DPSCs) in combination with appropriated scaffolds (β-TCP and GDPB) in a rat model of calvarial critical defect. We used μ-CT and PET analysis to quantify the potential increase in bone mineralization, either determining bone mineral density (BMD) or standard uptake 18F]-NaF value (SUV) after 2, 4, 8, and 12 weeks after the implant of the tissue-engineered constructs.

The results showed that: (1) β-TCP, either alone or in combination with DPSC, was completely absent or displaced from the defect area, (2) GDPB implants were mostly well positioned, with only two exception where the material inserted was displaced; (3) when comparing the two scaffolds, GDPB induced a higher amount of BMD and SUV within the cranial defect as compared to β-TCP, either alone or in combination with stem cells; (4) addition of stem cells to the grafts did not significantly induce an increase in BMD and SUV values as compared to the grafted scaffolds alone, although a small tendency to increase was observed.

The reason why we used micro-computed tomography is that μ-CT scans provide higher spatial and temporal

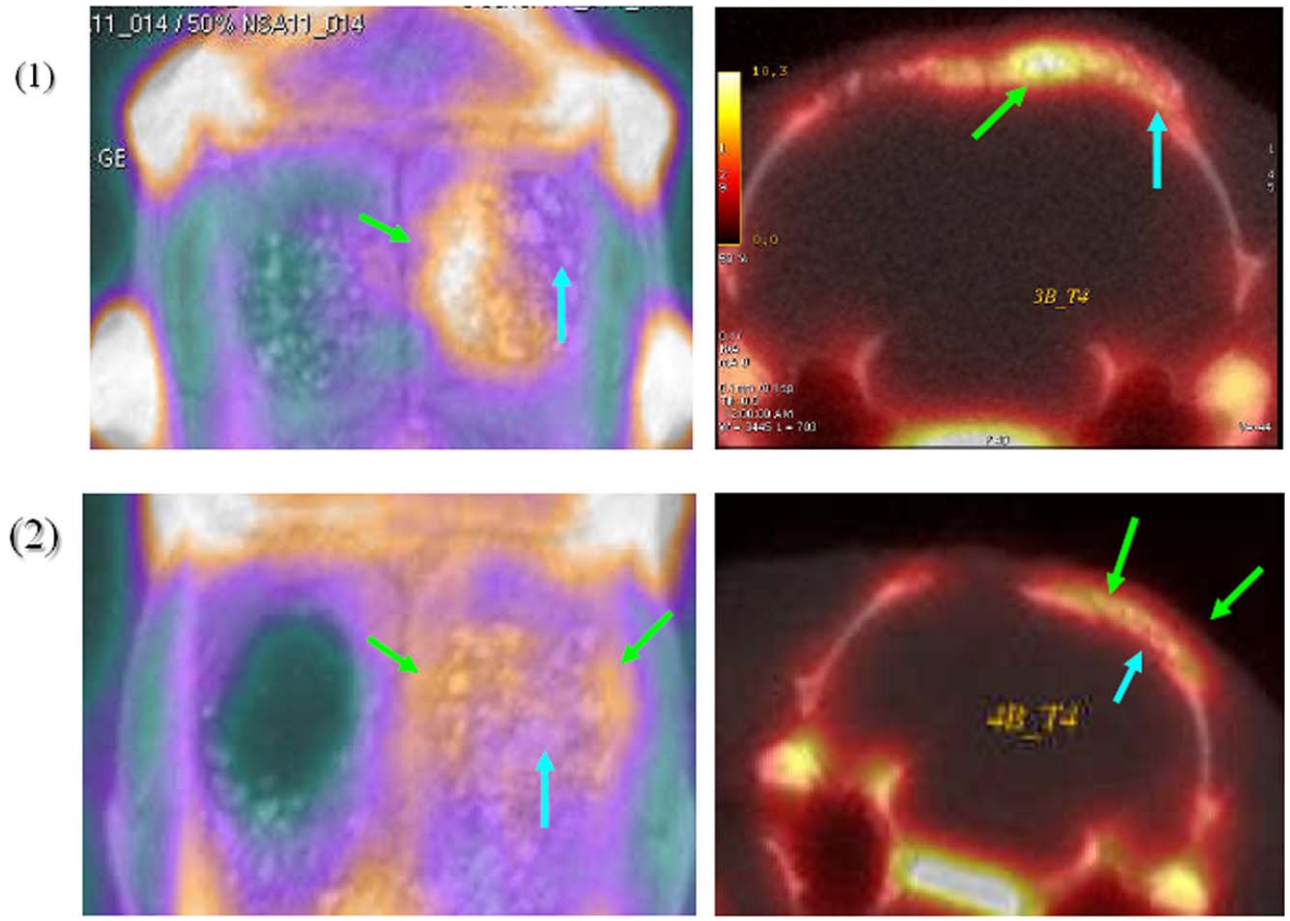

FIGURE 7. (1) 3D image (left side) and axial visualization (right side) of cranial defects of rat 3B after 4-weeks post-implant. Note the absence of homogeneity of PET signal into the defect. Strong signal (green arrow) on the defect border and weak signal (blue arrow) on the opposite side. (2) 3D image (left side) and axial visualization (right side) of cranial defects of rat 4B after 4-weeks post-implant. Note the strong PET signal (green arrow) on the defect border and weak signal (blue arrow) on the middle defect area. [Color figure can be viewed in the online issue, which is available at wileyonlinelibrary.com.]

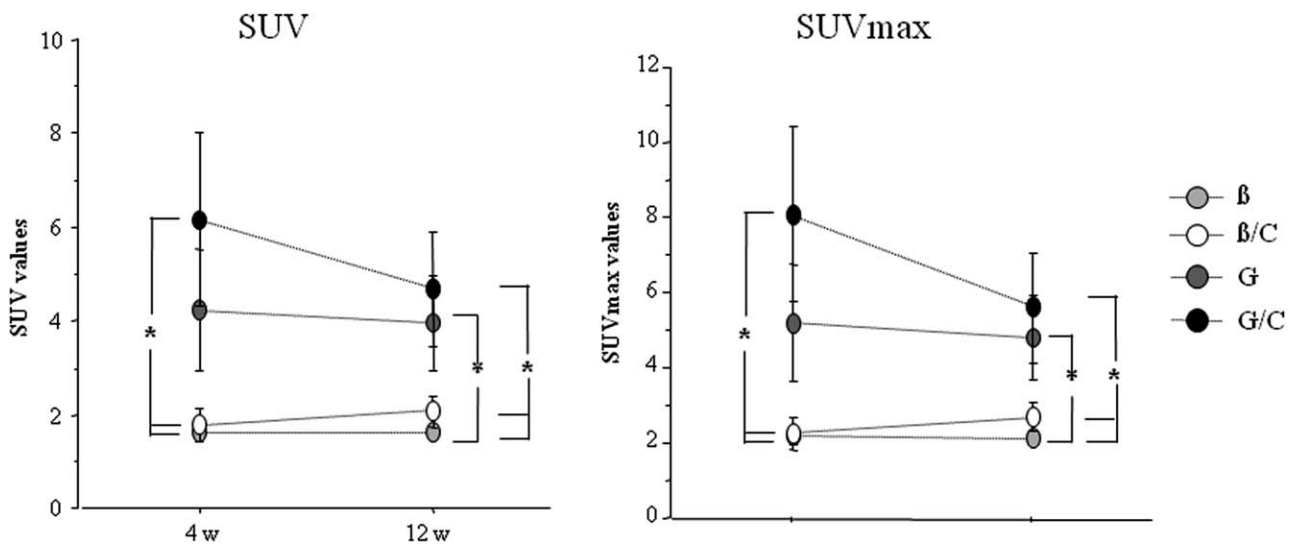

FIGURE 8. SUV and SUVmax mean values extrapolated from the quantitative analysis of images acquired at 4 and 12 weeks (w) from graft implant in the four experimental groups. β-TCP (β); β-TCP/DPSC (β/C); GDPB (G) and GDPB/DPSC (G/C). Data represent means ± S.E.M. β-TCP: Beta-tricalcium phosphate; GDPB: Granular deproteinized bovine bone; DPSC: dental pulp stem cells.

resolution imaging to capture detailed anatomical images of small animals.[33,34] Another reason consists in the possibility to quantify the increase in bone volume monitoring the progression within the same animal.[35] Moreover, the development of a rat imaging system that integrates positron emission tomography (PET) with x-ray computed tomography,[36] allowed the simultaneous anatomic and molecular imaging *in vivo* for precise measurements on bone microstructure.

The data obtained with multimodality PET/CT systems suggest that GDPB and ß-TCP provide different results when used in our model of tissue-engineered construct. The difference between them mainly consists in the fact that one is a biomaterial obtained by the deproteinization of bovine bone (GDPB)[37,38] while the other (ß-TCP) is a synthetic bone substitute that closely resembles natural bone in mineral composition.[39] Both of them have shown osteoconductive properties and are capable to provide a three-dimensional structure for bone regeneration.[40–43]

One important difference is that GDPB has lower level of resorbability[38,42] as compared to ß-TCP.[44] This property may be important because bone substitutes should be gradually absorbed and replaced by vital bone tissue, independently from the microenvironment of calvarial defect.[45] Thus one plausible hypothesis is that in our conditions the low level of resorbability of GDPB may favor bone formation as compared to β-TCP. This idea is supported by data obtained from previous studies. In a study of sinus augmentation it was shown that the deproteinized bovine bone induced an increased new bone formation as compared to β-TCP -based biomaterials.[46] On the other hand, β-TCP showed greater osteoconductivity and biodegradation properties than GDPB in a rat critical-size defect.[43]

Altogether these and our data indicate that optimal conditions favoring the process of osteogenesis may vary each time and may be dependent from several factors. These data suggest that local microenvironment generated by interactions among scaffolds, stem cells and native cells may interfere with osteogenic activity induced by the biomaterials and/or stem cells. At this regard, given that that GDPB is a biomaterial of natural origin it is probable that its higher biocompatibility may facilitate bone formation, either alone or in combination with stem cells. Another troubling factor with ß-TCP may be the excessive local concentration of calcium ions which causes osteoblastic cell death and dysfunction as a result of distorted cellular calcium metabolism.[47,48]

Our study also showed that addition of DPSC onto prewetted scaffolds did not substantially modify bone formation, although a tendency to increase BMD and SUV values was observed. This finding further support the idea that external factors may influence the fate of the cells. Among them, it has been shown that lack of appropriate differentiation factors[49] and/or the presence of pro-inflammatory mediators[50] may effectively reduce or stop the regeneration process. As mentioned before, in a previous experiment[22] where the same construct of scaffolds and stem cells were used, we found that tissue-engineered constructs did not significantly improve bone-induced regeneration process when compared to the effect of scaffolds alone. Also, no significant differences among scaffolds were found. In terms of tissue engineering, further research is required to increase the knowledge about optimal conditions for DPSC to induce bone regeneration. Future studies should focus on analysis of scaffolds that facility their integration, differentiation and matrix synthesis as well as on growth factors and signaling molecules implicated in bone regeneration.

There are some limitations to the interpretation of our data. First, the number of animals used in this study is insufficient to draw definitive conclusions. Second, the comparison between GDPB and ß-TCP BMD values may be not appropriated because β-TCP-based implants were not stable in the defect area. Third, we did not perform histological evaluations to determine the morphology and distribution of the cells in the scaffolds. For these reasons our observations must be regarded as preliminary data and additional studies are needed to determine the optimal conditions to induce bone regeneration in scaffold-based tissue-engineered constructs.

In summary, our micro-CT and Pet data, although at a preliminary level, indicate that GDPB, when used to fill critical calvarial defects, induces a greater percentage of bone formation as compared to β-TCP. Moreover, this study shows that addition of DPSC to the prewetted scaffolds has the potential to ameliorate bone regeneration process, although the set of optimal conditions requires further investigation.

ACKNOWLEDGMENTS

The authors thank Dr Alessia Caracci, Chair of Animal Facility and Preclinical Imaging—Nuclear Specialists Associated Srl (N.S.A) Ardea—Rome, Italy, for his assistance in micro-CT and PET evaluation.

REFERENCES

1. Bashutski JD, Wang HL. Periodontal and endodontic regeneration. J Endod 2009;35:321–328.
2. Ward BB, Brown SE, Krebsbach PH. Bioengineering strategies for regeneration of craniofacial bone: A review of emerging technologies. Oral Dis 2010;16:709–716.
3. Davies JE, Matta R, Mendes VC, Perri de Carvalho PS. Development, characterization and clinical use of a biodegradable composite scaffold for bone engineering in oro-maxillo-facial surgery. Organogenesis 2010;6:161–166.
4. Chen FM, Sun HH, Lu H, Yu Q. Stem cell-delivery therapeutics for periodontal tissue regeneration. Biomaterials 2012;33:6320–6344.
5. Holtorf HL, Jansen JA, Mikos AG. Modulation of cell differentiation in bone tissue engineering constructs cultured in a bioreactor. Adv Exp Med Biol 2006;585:225–241.
6. Bianco P, Robey PG. Stem cells in tissue engineering. Nature 2001;414:118–121.
7. Bruder SP, Kraus KH, Goldberg VM, Kadiyala S. The effect of implants loaded with autologous mesenchymal stem cells on the healing of canine segmental bone defects. J Bone Joint Surg Am 1998;80:985–996.
8. Bruder SP, Kurth AA, Shea M, Hayes WC, Jaiswal N, Kadiyala S. Bone regeneration by implantation of purified, culture-expanded human mesenchymal stem cells. J Orthop Res 1998;16:155–162.
9. Kon E, Muraglia A, Corsi A, Bianco P, Marcacci M, Martin I, Boyde A, Ruspantini I, Chistolini P, Rocca M, Giardino R, Cancedda R, Quarto R. Autologous bone marrow stromal cells loaded onto porous hydroxyapatite ceramic accelerate bone repair in

criticalsize defects of sheep long bones. J Biomed Mater Res 2000;49:328–337.
10. Cui L, Liu B, Liu G, Zhang W, Cen L, Sun J, Yin S, Liu W, Cao Y. Repair of cranial bone defects with adipose derived stem cells and coral scaffold in a canine model. Biomaterials 2007;28:5477–5486.
11. Yamada Y, Ueda M, Naiki T, Takahashi M, Hata K, Nagasaka T. Autogenous injectable bone for regeneration with mesenchymal stem cells and platelet rich plasma: Tissue-engineered bone regeneration. Tissue Eng 2004;10:955–964.
12. Meinel L, Fajardo R, Hofmann S, Langer R, Chen J, Snyder B, Vunjak-Novakovic G, Kaplan D. Silk implants for the healing of critical size bone defects. Bone 2005;37:688–698.
13. Mankani MH, Kuznetsov SA, Wolfe RM, Marshall GW, Robey PG. In vivo bone formation by human bone marrow stromal cells: Reconstruction of the mouse calvarium and mandible. Stem Cells 2006;24:2140–2149.
14. Miura M, Miura Y, Sonoyama W, Yamaza T, Gronthos S, Shi S. Bone marrow-derived mesenchymal stem cells for regenerative medicine in craniofacial region. Oral Dis 2006;12:514–522.
15. Kassem M, Risteli L, Mosekilde L, Melsen F, Eriksen EF. Formation of osteoblast-like cells from human mononuclear bone marrow cultures. APMIS 1991;99:269–274.
16. Cicconetti A, Sacchetti B, Bartoli A, Michienzi S, Corsi A, Funari A, Robey PG, Bianco P, Riminucci M. Human maxillary tuberosity and jaw periosteum as sources of osteoprogenitor cells for tissue engineering. Oral Surg Oral Med Oral Pathol Oral Radiol Endod 2007;104:618:e1–e12.
17. Li JH, Liu DY, Zhang FM, Wang F, Zhang WK, Zhang ZT. Human dental pulp stem cell is a promising autologous seed cell for bone tissue engineering. Chin Med J (Engl) 2011;124:4022–4028.
18. Yen AH, Yelick PC. Dental tissue regeneration—A mini-review. Gerontology 2011;57:85–94.
19. Zhang X, Naik A, Xie C, Reynolds D, Palmer J, Lin A, Awad H, Guldberg R, Schwarz E, O'Keefe R. Periosteal stem cells are essential for bone revitalization and repair. J Musculoskelet Neuronal Interact 2005;5:360–362.
20. Graziano A, d'Aquino R, Cusella-De Angelis MG, De Francesco F, Giordano A, Laino G, Piattelli A, Traini T, De Rosa A, Papaccio G. Scaffold's surface geometry significantly affects human stem cell bone tissue engineering. J Cell Physiol 2008;214:166–172.
21. Graziano A, d'Aquino R, Laino G, Papaccio G. Dental pulp stem cells: A promising tool for bone regeneration. Stem Cell Rev 2008;4:21–26.
22. Annibali S, Cicconetti A, Cristalli P, Giordano G, Ottolenghi L, Pilloni A. A comparative morphometric analysis of biodegradable scaffolds as carriers for dental pulp and periosteal stem cells in a model of bone regeneration. J Craniofacial Surg 2013;24:866–871.
23. Jones JR, Atwood RC, Poologasundarampillai G, Yue S, Lee PD. Quantifying the 3D macrostructure of tissue scaffolds. J Mater Sci Mater Med 2009;20:463–471.
24. Neiva R, Pagni G, Duarte F, Park CH, Yi E, Holman LA, Giannobile WV. Analysis of tissue neogenesis in extraction sockets treated with guided bone regeneration: Clinical, histologic, and micro-CT results. Int J Periodontics Restorative Dent 2011;3:457–469.
25. Vasquez SX, Shah N, Hoberman AM. Small animal imaging and examination by micro-CT. Methods Mol Biol 2013;947:223–231.
26. Ruggiu A, Tortelli F, Komlev VS, Peyrin F, Cancedda R. Extracellular matrix deposition and scaffold biodegradation in an in vitro three-dimensional model of bone by X-ray computed microtomography. J Tissue Eng Regen Med 2012.
27. Cartmell S, Huynh K, Lin A, Nagaraja S, Guldberg R. Quantitative microcomputed tomography analysis of mineralization within three-dimensional scaffolds in vitro. J Biomed Mater Res A 2004; 69A:97–104.
28. Phelps ME. PET: The merging of biology and imaging into molecular imaging J Nucl Med 2000;41:661–681.
29. Gronthos S, Mankani M, Brahim J, Gehron Robey P, Shi S. Postnatal human dental pulp stem cells (DPSCs) in vitro and in vivo. Proc Natl Acad Sci 2000;97:13625–13630.
30. Karaöz E, Doğan BN, Aksoy A, Gacar G, Akyüz S, Ayhan S, Genç ZS, Yürüker S, Duruksu, G, Demircan PÇ, Sariboyaci AE. Isolation and in vitro characterization of dental pulp stem cells from natal teeth. Histochem Cell Biol 2010;133:95–112.
31. Mafi P, Hindocha S, Mafi R, Griffin M, Khan WS. Adult mesenchymal stem cells and cell surface characterization—A systematic review of the literature Open Orthop J 2011;5 (Suppl 2):253–260.
32. Mangano C, De Rosa A, Desiderio V, D'Aquino R, Piattelli A, De Francesco F, Tirino V, Mangano F, Papaccio G. The osteoblastic differentiation of dental pulp stem cells and bone formation on different titanium surface textures. Biomaterials 2010;31:3543–3551.
33. Umoh JU, Sampaio AV, Welch I, Pitelka V, Goldberg HA, Underhill TM, Holdsworth DW. In vivo micro-CT analysis of bone remodeling in a rat calvarial defect model. Phys Med Biol 2009; 54:2147–2161.
34. Schambach SJ, Bag S, Schilling L, Groden C, Brockmann MA. Application of micro-CT in small animal imaging. Methods 2010; 50:2–13.
35. Snoeks TJ, Kaijzel EL, Que I, Mol IM, Löwik CW, Dijkstra J. Normalized volume of interest selection and measurement of bone volume in microCT scans. Bone 2011;49:1264–1269.
36. Goertzen AL, Meadors AK, Silverman RW, Cherry SR. Simultaneous molecular and anatomical imaging of the mouse in vivo. Phys Med Biol 2002;47:4315–4328.
37. Berglundh T, Lindhe J. Healing around implants placed in bone defects treated with Bio-Oss. Clin Oral Implants Res 1997;8:117–124.
38. Piattelli M, Favero GA, Scarano A, Orsini G, Piattelli A. Bone reactions to anorganic bovine bone (Bio-Oss) used in sinus lifting procedure: A histologic long-term report of 20 cases in man. Int J Oral Maxillofac Implants 1999;14:835–840.
39. LeGeros RZ. Properties of osteoconductive biomaterials: Calcium phosphates. Clin Orthop Relat Res 2002;395:81–98.
40. Sánchez-Salcedo S, Nieto A, Gómez-Barrena E, Vallet-Regí M. Hydroxyapatite/β-tricalcium phosphate/agarose macroporous scaffolds for bone tissue engineering. Chem Eng J 2008;137:62–71.
41. Nguyen LT, Liao S, Chan CK, Ramakrishna S. Enhanced osteogenic differentiation with 3D electrospun nanofibrous scaffolds. Nanomedicine (Lond) 2012;7:1561–1575.
42. Valentini P, Abensur D. Maxillary sinus floor elevation for implant placement with demineralized freeze-dried bone and bovine bone (Bio-Oss): A clinical study of 20 patients. Int J Periodontics Restorative Dent 1997;17:233–241.
43. Kato E, Lemler J, Sakurai K, Yamada M. Biodegradation property of beta-tricalcium phosphate-collagen composite in accordance with bone formation: A comparative study with bio-oss collagen® in a rat critical-size defect model. Clin Implant Dent Relat Res 2012 Jul 18. [Epub ahead of print].
44. Borrelli J Jr, Prickett WD, Ricci WM. Treatment of nonunions and osseous defects with bone graft and calcium sulfate. Clin Orthop Relat Res 2003;411:245–254.
45. Park CH, Rios HF, Jin Q, Sugai JV, Padial-Molina M, Taut AD, Flanagan CL, Hollister SJ, Giannobile WV. Tissue engineering bone-ligament complexes using fiber-guiding scaffolds. Biomaterials 2012;33:137–145.
46. Simunek A, Kopecka D, Somanathan RV, Pilathadka S, Brazda T. Deproteinized bovine bone versus beta-tricalcium phosphate in sinus augmentation surgery: A comparative histologic and histomorphometric study. Int J Oral Maxillofac Implants 2008;23:935–942.
47. Link DP, van den Dolder J, Wolke JG, Jansen JA. The cytocompatibility and early osteogenic characteristics of an injectable calcium phosphate cement. Tissue Eng 2007;13:493–500.
48. Saunders R, Szymczyk KH, Shapiro IM, Adams CS. Matrix regulation of skeletal cell apoptosis III: Mechanism of ion pair-induced apoptosis. J Cell Biochem 2007;100:703–715.
49. Osugi M, Katagiri W, Yoshimi R, Inukai T, Hibi H, Ueda M. Conditioned media from mesenchymal stem cells enhanced bone regeneration in rat calvarial bone defects. Tissue Eng A 2012;18: 1479–1489.
50. Liu Y, Wang L, Kikuiri T, Akiyama K, Chen C, Xu X, Yang R, Chen W, Wang S, Shi S. Mesenchymal stem cell-based tissue regeneration is governed by recipient T lymphocytes via IFN-γ and TNF-α. Nat Med 2011;17:1594–1601.